Si–O barrier technology for bacterial cellulose nanocomposite flexible displays

S. Ummartyotin [a], J. Juntaro [b], M. Sain [b,*], H. Manuspiya [a,**]

[a] The Petroleum and Petrochemical College, Center of Excellence for Petroleum, Petrochemicals and Advanced Materials Chulalongkorn University, Bangkok 10330, Thailand
[b] Centre for Biocomposites and Biomaterials Processing, Faculty of Forestry, University of Toronto, 33 Willcocks Street, Toronto M5S 3B3, Canada

ARTICLE INFO

ABSTRACT

Si–O thin film was successfully deposited on bacterial cellulose nanocomposite via plasma enhanced chemical vapor deposition (PECVD) as transparent barrier against water vapor. X-ray photoelectron spectroscopy (XPS) confirmed consistent Si and O atomic concentrations through the entire depth of the Si–O layer. The Si–O layer had uniform and highly smooth surface – more than 80% of the surface features the surface roughness of 15 nm. The water vapor transmission rate (WVTR) of the bacterial cellulose nanocomposite was evaluated as 9×10^{-2} g/m^2/day, but after the deposition of the Si–O barrier layer, the WVTR in the range of 10^{-4} g/m^2/day was achieved. The WVTR property of the nanocomposite can be further adjusted through the operating parameters of PECVD. These properties indicated the quality of the Si–O film as an effective water vapor barrier. Bacterial cellulose nanocomposite deposited with Si–O barrier film can be useful as substrate for flexible organic light emitting diode (OLED) displays.

© 2011 Elsevier Ltd. All rights reserved.

1. Introduction

The rapid growth of optoelectronic technology and flexible electronic materials has been evident in the past decade. Among the electronic displays, organic light emitting diode (OLED), with the features of low power consumption, wide viewing angle and excellent contrast, is a versatile platform system that has attracted worldwide attention (Geffroy et al., 2006). Although OLED has traditionally been fabricated on rigid glass sheet substrates, flexible polymeric materials have recently emerged as promising alternatives (Auch et al., 2002; Legnani et al., 2008; Okahisa et al., 2009; Yang et al., 2007). Through the achievement of flexible OLED, next generation flexible TV screen, flexible computer screen, and other flexible display systems will be one step closer to our daily lives. Several literatures regarded cellulose-based nanocomposite as a potential substrate for flexible displays (Legnani et al., 2008; Nogi and Yano, 2008; Okahisa et al., 2009; Wu, 2010). Such material features novel concept of display device with environmentally friendly aspect. Other benefits include acceptable mechanical properties, transparency, light weight, and ultra high dimensional stability in a wide range of temperature. Its flexibility will facili-

tate the mass production of printed electronics through roll-to-roll (RTR) process (Lee et al., 2010; Noh et al., 2010). However, one limitation of cellulose-based nanocomposites in electronics application is the hydrophilic nature of cellulose. Electronic devices, especially OLED, is highly sensitive to moisture. For an OLED lifetime of >10,000 h, the low water vapor transmission rate (WTVR) of 10^{-6} g/m^2/day is required (Choi et al., 2008; Lewis and Weaver, 2004). Water vapor can oxidize metallic cathode and active organic materials, and thus drastically reduce the lifetime and efficiency of OLED. In order to overcome this issue, various barrier technologies have been investigated (Choi et al., 2008; Lewis, 2006; Lewis and Weaver, 2004). The critical challenge lies in the creation of barrier material that offers flexibility and optical transparency. The reflective index (RI) of the barrier must also match that of the nanocomposite, as mismatching RI will disrupt the transparency of the OLED substrate. In this work, we tackle the barrier challenge by coating the bacterial cellulose OLED substrate with Si–O layer. Optically transparent Si–O barrier film with the thickness in nano-scale was deposited through plasma enhanced chemical vapor deposition (PECVD). Si–O film prepared through this technique offers the epitaxial crystal growth on surface with excellent uniformity and adherence to the substrate (Borer et al., 2006; Borer and Rohr, 2005; Kim et al., 2002; Techima et al., 2001). PECVD uses the ion bombardment on the surface, allowing the possibility of depositing high film quality at low temperature (Tendero et al., 2006). Consequently the thermal degradation of the polymeric substrate can be restricted to minimal. The preparation of nanocomposite substrate, composed

* Corresponding author. Tel.: +1 416 9463191; fax: +1 416 978 3834.
** Corresponding author. Tel.: +66 2 2184101; fax: +66 2 215 4459.
E-mail addresses: m.sain@utoronto.ca (M. Sain), hathaikarn.m@chula.ac.th (H. Manuspiya).

of nano-scale cellulose and polyurethane resin, was reported elsewhere (Wu, 2010). In this article, deposition of Si–O layer, and its surface characterizations through Fourier-transformed infrared spectroscopy (FTIR), X-ray photoelectron spectroscopy (XPS), and atomic force microscope (AFM) are reported. The barrier performance was consequently investigated in terms of WVTR.

2. Experimental

2.1. Nano-scale barrier film preparation

Si–O film was deposited on nanocomposite substrate via PECVD in a parallel plate, capacitively coupled-plasma (13.56 MHz) reactor with an electrode spacing of 4 cm. A gas showerhead, which was electrically isolated from the reactor by a ceramic spacer, acted as the power electrode. On the grounded electrode, a ceramic heater capable of heating up to 400 °C was used to heat the substrate. The substrate temperature was measured by the thermocouple tube which was electrically shielded from plasma. The thermocouple tube was in contact with the backside of the substrate holder. SiH_4 (5%) in O_2 was used as a source gas. During the epitaxial growth process, the N_2 gas flow rate was maintained at 100 sccm. PECVD was conducted at 130 °C in order to prevent any thermal deformation of nanocomposite substrate. The deposition rate was set at 25 nm/min. Three deposition times were attempted – 2, 4 and 8 min; therefore, Si–O layer with the estimated thickness of 50, 100 and 200 nm were expected to be deposited on nanocomposites. From hereon, the bacterial cellulose nanocomposite deposited with Si–O layer with the estimated thickness of 50, 100 and 200 nm, will be referred to as ∼50 nm-thick sample, ∼100 nm-thick sample and ∼200 nm-thick sample respectively.

2.2. Nano-scale barrier film characterization

2.2.1. Ellipsometer

Spectroscopic ellipsometer (M-44 ellipsometer, J.A. Woollam, NE, USA) equipped with silicon carbide plate for controlling position was used to determine the refractive index (RI) of nanocomposites at ambient temperature. The instrument had a variable angle stage, allowing adjustment of the incident angle. It performed on a rotating polarizer principle, in which the polarization of the incident light was varied. Reflected intensity was recorded with a grating charged-coupled device (CCD) over the wavelength of 400–900 nm. The measurements were repeated 5 times. Subsequent curve fitting allowed for the determination of refractive index and its variation with wavelength.

2.2.2. Attenuated total reflectance-Fourier transform infrared spectroscopy (ATR-FTIR)

ATR-FTIR was performed on a Bruker Vector 22 mid-IR spectroscopy (Bruker, Germany), equipped with an ATR crystal (50 mm × 10 mm × 2 mm) at 45° incident angle configuration. All FTIR absorption spectra were recorded over 4500–500 cm^{-1} wavenumbers region at a resolution of 8 cm^{-1} with 1024 scans using a deuterated triglycine sulfate (DTGS) detector. A straight line between two lowest points in the respective spectra region was chosen as a baseline. The position of Si–O region was taken from literature (Hu et al., 2003).

2.2.3. X-ray photoelectron spectroscopy (XPS)

XPS was performed using Thermo Scientific ESCALAB 250Xi XPS spectrometer (Thermo Fisher Scientific Inc., MA, USA) with a monochromatic Al-Kα X-ray source. The spot size for analysis was approximately 400 μm. Samples were analyzed at 90° take off angle with respect to the surface. A low resolution survey spectrum ranging from 0 to 1300 eV was conducted at 150 eV pass energy. To
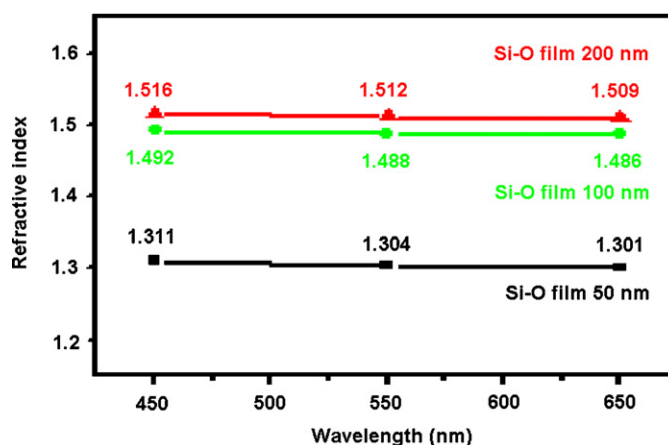

Fig. 1. Refractive indices of nanocomposites after the deposition of Si–O layer at difference thicknesses.

determine the relative atomic percentage, high-resolution spectra in the ranges of 150–200 eV, 280–300 eV and 520–530 eV binding energy were obtained for Si1s, C1s and O1s region, respectively. The bond and depth profile analysis was determined by curve fitting. The data was analyzed using Avantage onboard software supplied by Thermo Scientific with the instrument.

2.2.4. Atomic force microscope (AFM)

AFM was performed with a Digital Instruments Nanoscope III Scanning Probe Microscope (Digital Instruments, CA, USA) in ambient conditions (22 °C, 45–55% relative humidity) over areas of 25 μm × 25 μm at the normal load ranging from 5 nN to 130 nN at a scan rate of 0.5 Hz (resulting a scanning speed of 2 μm/s). Square pyramidal Si_3N_4 tips with a nominal 30–50 nm radius mounted on triangular Si_3N_4 cantilevers with a spring constant of 0.58 N/m were used. Adhesive forces were determined from the force calibration plot (FCP).

2.2.5. Water vapor transmission rate (WVTR)

WVTR was measured in accordance with ASTM E96-66 standard. The controlled environment inside a closed desiccator was maintained at 50 ± 2% relative humidity throughout the experiment by a saturated aqueous solution of $Ca(NO_3)_2$, which will control the humidity to be 51% at 24.5 °C. The experiment was performed at room temperature (25 °C). Sample thickness was approximately 2.0–2.5 mm. The dried sample from the oven was put in the desiccator for at least 2 h prior to the experiment to equilibrate the sample with the atmospheric moisture inside. Demineralized water was put into a permeability Payne cup (2.5 cm diameter). The water level was kept at least 2 cm from the sample to avoid contact between the sample and the water. The sample was then attached to the Payne cup. The sample weight change as a function of time was monitored everyday for 2 weeks. The WVTR was calculated as:

$$WVTR = \frac{G}{tA}$$

where G is the gain weight, t is the time and A is the test area.

3. Results and discussion

3.1. Ellipsometry

The refractive index (RI) of the nanocomposites after the deposition of Si–O layer was measured as shown in Fig. 1. The samples with the estimated thickness of 100 nm and 200 nm of Si–O layers exhibited RI in the range of 1.486–1.516 in the light wavelength of
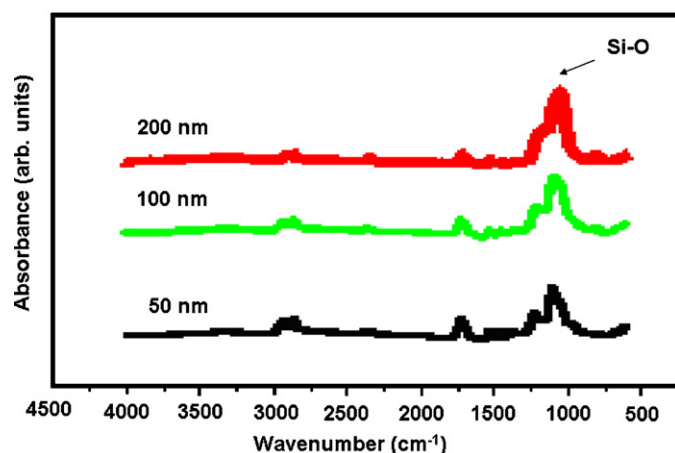
Fig. 2. ATR-FTIR spectra of Si–O film deposited via PECVD process.

Fig. 3. XPS survey spectra for Si–O layer deposited on bacterial cellulose nanocomposite.

450–650 nm. In comparison, the RI of cellulose has been reported as 1.618 along the fiber axis and 1.544 in the transverse direction (Nogi and Yano, 2008; Sperling, 2001), suggesting that the RI of cellulose was only slightly affected by the fabrication of nanocomposites and the deposition of Si–O layer. The nanocomposite with ~50 nm of Si–O layer however exhibited different RI, which can be ascribed to the unsuccessful deposition of Si–O layer, as will be discussed in Section 3.3. All nanocomposites appeared optically transparent after PECVD. Fig. 1 also reveals that for all samples, RI decreases as the wavelength increases – such relationship complies well with the Cauchy relation (Born and Wolf, 1999).

3.2. Attenuated total reflectance-Fourier transform infrared spectroscopy (ATR-FTIR)

ATR-FTIR was performed to detect the Si–O layer that was deposited on the nanocomposites. The IR absorption characteristic of Si–O has been studied; three major absorption bands centered at 460, 810, and 1070 cm^{-1} have been confirmed by many researchers (Kirk, 1988). These three absorption peaks reflect the rocking of an oxygen atom about an axis through the two silicon, the symmetrical stretching of an oxygen atom along a line bisecting the axis through the two silicon atoms and asymmetrical stretching of an oxygen atom along a line parallel to the axis through the two silicon atoms, respectively (Hu et al., 2003). According to Fig. 2, absorption peaks centered at 810 and 1070 cm^{-1} can be observed in all samples, confirming the quality of Si–O layer.

3.3. X-ray photoelectron spectroscopy (XPS)

XPS was performed to determine the atomic composition of the Si–O barrier film. Low resolution XPS survey spectra revealed that the main elements present on the surface of the deposited nanocomposites were carbon, oxygen and silicon (Fig. 3). The XPS spectra for ~100 nm-thick and ~200 nm-thick samples show Si peak in the region of 100–120 eV, suggesting the successful deposition of the silicon-based layer. However, the XPS spectrum of the ~50 nm-thick sample does not show the Si peak, suggesting that the deposition time was not sufficient for the effective formation of Si–O thin layer.

As high resolution XPS was performed in the Si1s region, of which the peaks correspond to the binding energy at 104 eV following XPS spectral line database of National Institute of Standard and Technology (NIST), USA, the peaks revealed that Si content at the surface of ~100 nm-thick and ~200 nm-thick samples were not
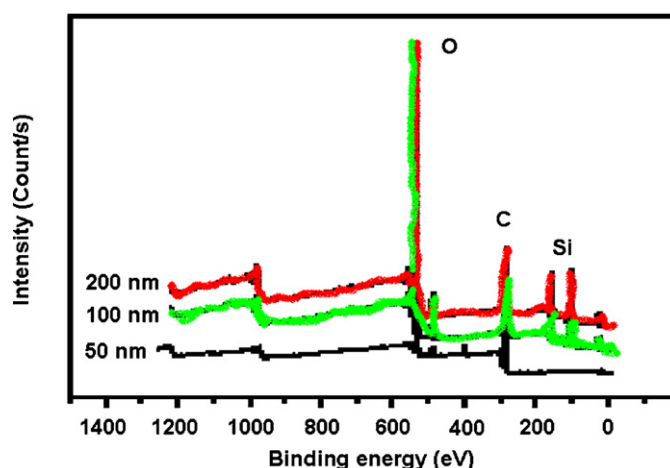
significantly different, and that the ~50 nm-thick sample did not have Si content (Fig. 4).

To investigate the Si–O atomic concentration as a function of depth for all Si–O deposited nanocomposites, the depth profile analysis was carried out by 4 keV Ar$^+$ etching technique (Fig. 5). It can be observed that the surface atomic compositions of the top layer (i.e., at 0 nm depth) of all samples were different from the composition at the adjacent level. Here the 0 nm-depth composition profiles in Fig. 5 corresponds to the surface concentrations of the Si–O thin film after 1 min of Ar$^+$ sputtering, which was required for cleaning purpose. In general, prolonged Ar$^+$ bombardment can lead to significant chemical changes in the film surface. In this case, the Ar$^+$ sputtering led to a preferential loss of Si and O.

The concentration profile of the ~50 nm-thick sample showed no content of Si (Fig. 5a), which is in agreement with earlier results. The atomic concentration profile consequently belonged to the bacterial cellulose nanocomposite. In the case of ~100 nm-thick and ~200 nm-thick samples (Fig. 5b and c), similar and consistent atomic composition profiles of the Si–O bulk layers were obtained. Here Si is in its metallic state without apparent oxidation from the Ar$^+$ bombardment. Both ~100 nm-thick and ~200 nm-thick samples exhibited similar Si concentration of 37–40% and O concentration of 57–59%. The Si and O concentration of the ~100 nm-thick sample dropped drastically as the depth reached 70–90 nm, while in the case of the ~200 nm-thick sample, the drop was observed at the depth of 150–170 nm. Such abrupt changes in the film composition indicated the interface region between the
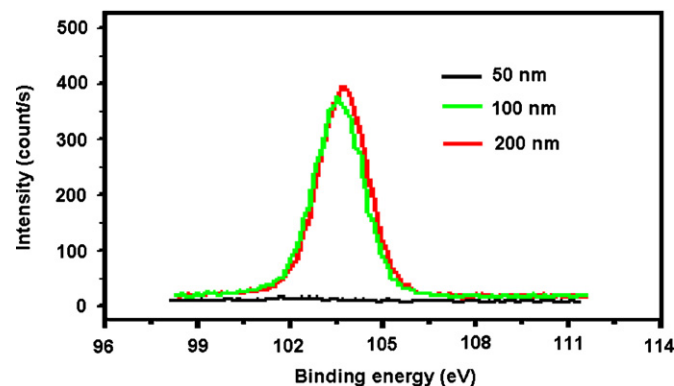

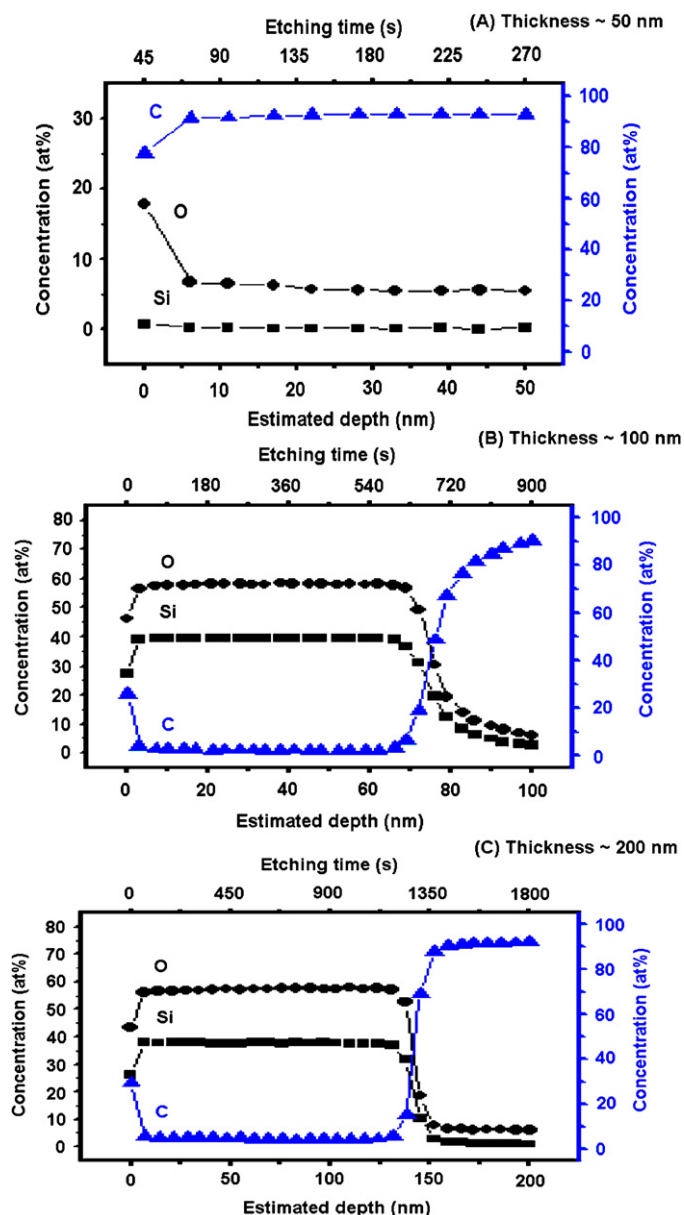**Fig. 4.** High resolution XPS peak of Si1s region of Si–O layer deposited on bacterial cellulose nanocomposite.

Fig. 5. Depth profile analysis of Si–O deposited bacterial cellulose nanocomposite (A) thickness ~50 nm, (B) thickness ~100 nm and (C) thickness ~200 nm.

Fig. 6. Top view AFM image of (a) bacterial cellulose sheet and (b) nanocomposite.

Si–O layer and the nanocomposite substrate. Depth profile analysis beyond these interface regions did not detect any trace of Si.

3.4. Atomic force microscope (AFM)

Fig. 6 illustrates AFM image taken with lateral contact mode. In this work, ten AFM images were taken at different areas on the sample, all of which revealed comparable topologies. The AFM scan size (25 μm × 25 μm) implied the uniformity of the surface roughness. It is obvious that the smoothness of the bacterial cellulose sheet was immensely improved after the impregnation of polyurethane resin (Fig. 6). The sheet roughness reduced from 1.162 μm to 81 nm as the micron-scale pores of the bacterial cellulose sheet was filled with the resin. Additional information of cellulose nanocomposite preparation, characterization and scientific properties has been discussed elsewhere (Wu, 2010).After the nanocomposite was deposited with ~100 nm-thick Si–O layer, the AFM image shows that the substrate surface was covered with Si–O
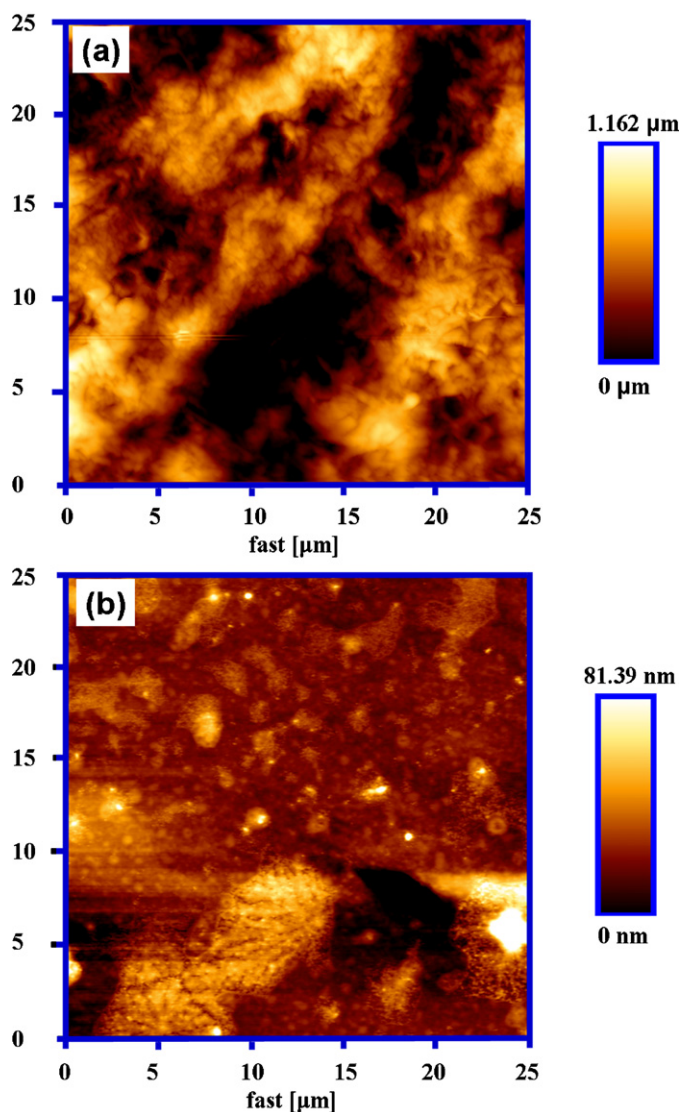
crystallite (Fig. 7). The epitaxial growth of the crystallite yielded the uniform topology with the roughness of ~62 nm, which was also a significant improvement over the surface roughness of the pre-deposited nanocomposite. Part of the image, indicated as the green line, was sampled from the relatively smooth area, which represented more than 80% of the whole AFM image, for the Fourier transformed pattern analysis (Tomita et al., 1985) – an alternative analysis proposed to facilitate the assessment of 2D surface morphology. This technique involved a statistical analysis to derive statistical parameters which are correlated with surface roughness. In this case, the length of the green line is 11.25 μm and the average surface roughness is ~15 nm, suggesting the exceptionally smooth surface of most part (>80%) of Si–O barrier film. Its roughness was only slightly higher than the specification for OLED substrate, as suggested by Choi et al. (2008) (<5 nm).

The adhesive force of the Si–O barrier layer was also measured through FCP technique. The FCP curve for the 100 nm-thick Si–O deposited sample is shown in Fig. 8 as an example. In this technique, the AFM tip was brought into contact with the sample while the maximum force needed to pull the tip and the sample apart was measured. As the tip approached the sample within a few nanometers (point A in Fig. 8), an attractive force existed between the atoms of the tip surface and atoms of the sample surface. The tip was
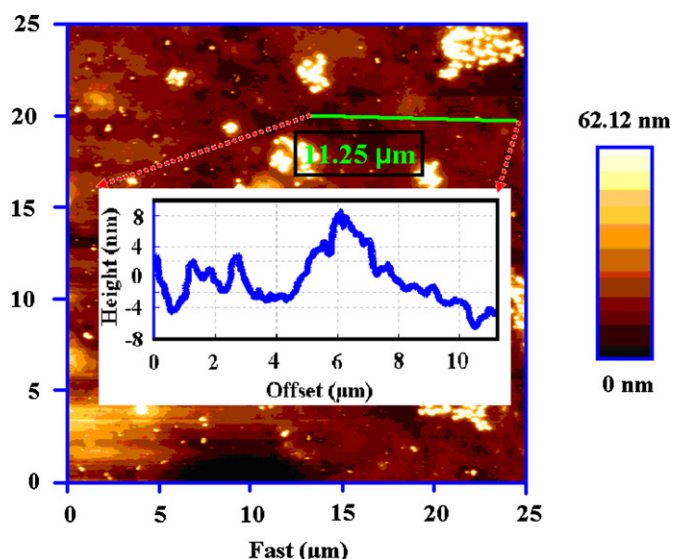
Fig. 7. Top view AFM image of Si–O barrier deposited on cellulose nanocomposite substrate with Fourier transformed pattern.

Table 1
WTVR properties of the nanocomposites in comparison to the OLED requirement and conventional polymers.

	WVTR (g/m^2/day)
Bacterial cellulose nanocomposite	0.09
100, 200 nm Si–O deposited nanocomposite	$\sim 10^{-4}$
Requirement for OLEDs (Choi et al., 2008)	$\sim 10^{-6}$
Polyethylene (Lewis and Weaver, 2004)	1.2–5.9
Polystyrene (Lewis and Weaver, 2004)	7.9–40

(Liew et al., 2000; Papadimitrakopoulos et al., 1998). The widely quoted requirement for WTVR for an OLED life time of more than 10,000 h has been reported as 1×10^{-6} g/m^2/day (Choi et al., 2008). Traditionally, barrier thin films are made of oxide of Al or Si. They are effectively impermeable to oxygen and water (Barrer, 1941). In this work, after the nanocomposite was deposited with Si–O layer, its moisture barrier performance was greatly enhanced. Table 1 shows the WVTR properties of the nanocomposite before and after the Si–O deposition, in comparison to the OLED requirement and conventional polymers. Si–O layer can effectively cover the substrate roughness and fill the pinholes, reducing WVTR down to the order of 10^{-4} g/m^2/day. The nanocomposite deposited with Si–O layers with the thickness of 100 nm and 200 nm exhibited WVTR performance in the same range, suggesting that water vapor permeation occurred through defects or nanoscale pinholes, rather than the bulk of the Si–O layer.

Many governing factors exist in Si–O PECVD, including deposition time, RF power, pressure, gas flowrate and plasma stabilization. These parameters will ultimately affect coating properties such as uniformity, thickness and density. Coating properties can be improved with deposition power, as increasing deposition power will enhance excitation and dissociation of Si(H$_4$) and O$_2$ molecules in the plasma. Heat can also improve the mobility of the active species and thus expedites crosslinking of the Si–O network, eliminating the porous defects (Choi et al., 2008). As the WVTR performance of the Si–O deposited nanocomposite in this work was still two orders of magnitude short of the OLED requirement, in the following section, the effects of deposition pressure and RF power on the WVTR performance are investigated.

The WVTR of ~ 100 nm-thick Si–O deposited nanocomposites fabricated at different deposition pressures is demonstrated in Fig. 9. It can be observed that WVTR can be improved by increasing the deposition pressure. Increasing the deposition pressure will decrease the kinetic energy of the active species, as their residence time in the gas phase will be longer, and led to the formation of Si–O barrier layer with lower residual stress. Consequently fewer

then pulled toward the sample, and contact occurred at point B. In general, the adsorption of water molecules on the sample surface could also accelerate this so-called "snap-in", due to the formation of water around the tip. As the piezo extended further, the cantilever further deflected, which was represented by the slope portion of the curve. As the piezo retracted, at point C the tip went beyond the zero deflection because of the attractive forces, into the adhesive force region. At point D, the tip snapped free of the adhesive force and was consequently in free air. Therefore, the adhesive force was determined by multiplying the cantilever spring constant (0.58 N/m) by the horizontal distance between point C and D, which corresponded to the maximum cantilever deflection toward the samples before the tip was disengaged. Our Si–O barrier film with estimated thickness of 50, 100 and 200 nm revealed the adhesion force in the range of 116–174 nN.

3.5. Water vapor transmission rate (WVTR)

OLED is extremely sensitive to moisture. In presence of moisture, the reactive low work function metals used as cathodes can delaminate from the underlying organic layer, while commonly used organic materials can form non-emissive quenching species
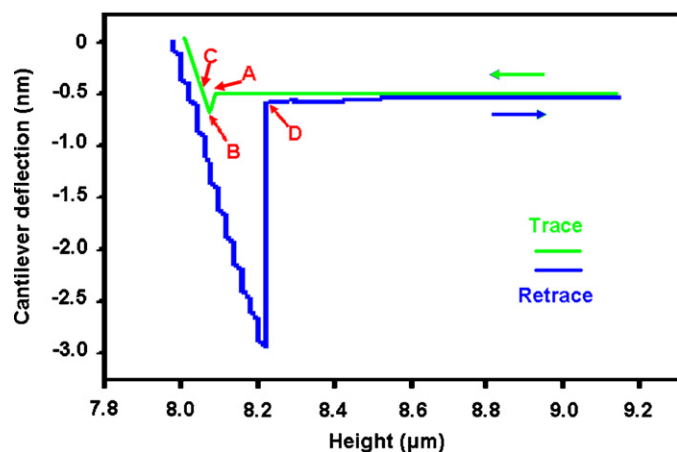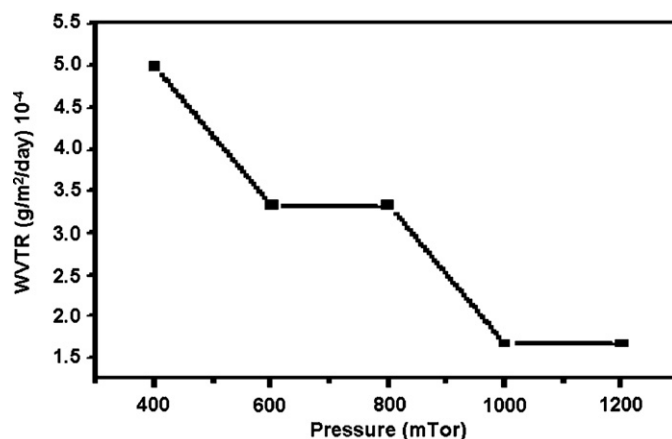

Fig. 8. Typical FCP of ~ 100 nm-thick Si–O barrier deposited on cellulose nanocomposite substrate in ambient air.

Fig. 9. WVTR of ~ 100 nm-thick Si–O deposited on cellulose nanocomposite substrate versus deposition chamber pressure.
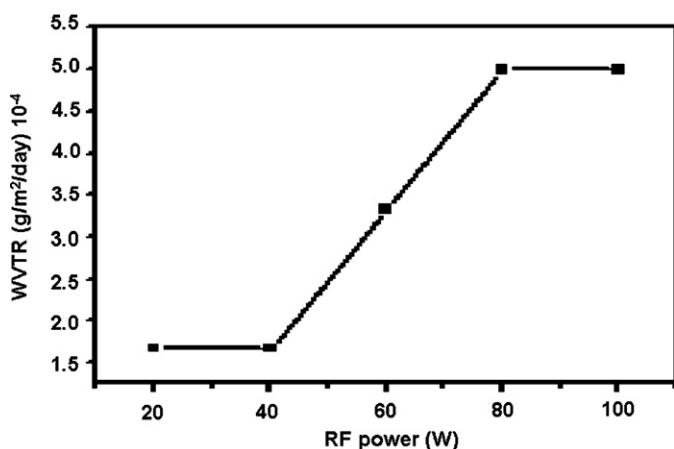
Fig. 10. WVTR of ~100 nm-thick Si–O deposited on cellulose nanocomposite substrate versus RF power.

defects, including nano-crack and pinhole, can be obtained. Higher pressure can also induce larger Si–O particles and more stable bonding at the surface of particles (Wuu et al., 2004). Fig. 10 exhibits the influence of the RF power on WVTR of ~100 nm-thick Si–O deposited nanocomposite fabricated at the deposition pressure of 1000 mTorr. It can be observed that lower RF power is preferred for higher moisture barrier property. When RF power is increased, higher amount of active oxygen gas is generated (da Silva et al., 2000), leading to the formation of Si–O barrier layer with higher residual stress and therefore more defects. Higher RF power will also lead to rougher surface (Wuu et al., 2004).

This preliminary work exhibited that Si–O film deposited by PECVD was successfully carried out, and that adjusting PECVD parameters can improve the water vapor barrier property of the Si–O layer. Nevertheless, as OLED is extremely sensitive to moisture, the WVTR is still 100 times higher than the specification for OLED substrate. More effective barrier performance of Si–O layer still needs to be further developed for the application of OLED substrate.

4. Conclusion

Si–O layer was successfully deposited on bacterial cellulose nanocomposite through PECVD. The transparency and flexibility of the nanocomposite were retained. The deposited Si–O layer offered uniform and exceptionally smooth surface. Most of the surface had the roughness of 15 nm. WVTR results revealed that Si–O layer with the thickness of ~100 nm had barrier property comparable to that with the thickness of ~200 nm. Si–O deposition can reduce the WVTR down to 10^{-4} g/m^2/day. However, the barrier performance of Si–O layer still needs development to achieve the specification for OLED substrate of 10^{-6} g/m^2/day (Choi et al., 2008).

References

Auch, M. D. J., Soo, O. K., Ewald, G., & Jin, C. S. (2002). Ultrathin glass for flexible OLED application. *Thin Solid Films, 417*, 47–50.
Barrer, R. M. (1941). *Diffusion in and through solids*. New York: Cambridge University Press.
Borer, B., & Rohr, R. V. (2005). Growth structure of SiO$_x$ films deposited on various substrate particles by PECVD in a circulating fluidized bed reactor. *Surface and Coatings Technology, 200*, 377–381.
Borer, B., Sonnenfeld, A., & Rohr, R. V. (2006). Influence of substrate temperature on morphology of SiO$_x$ films deposited on particles by PECVD. *Surface and Coatings Technology, 201*, 1757–1762.
Born, M., & Wolf, E. (1999). *Principles of optics: electromagnetic theory of propagation, interference and diffraction of light*. Cambridge: Cambridge University Press.
Choi, M. C., Kim, Y., & Ha, C. S. (2008). Polymers for flexible displays: From material selection to device application. *Progress in Polymer Science, 33*, 581–630.
da Silva, A. N. R., Morimoto, N. I., & Bonnaud, O. (2000). Tetraethylorthosilicate SiO$_2$ films deposited at a low temperature. *Microelectronics Reliability, 40*(4–5), 621–624.
Geffroy, B., Le Roy, P., & Prat, C. (2006). Review Organic light-emitting diode (OLED) technology: Materials, devices and display technologies. *Polymer International, 55*, 572–582.
Hu, Q., Suzuki, H., Gao, H., Araki, H., Yang, W., & Noda, T. (2003). High-frequency FTIR absorption of SiO$_2$/Si nanowires. *Chemical Physics Letters, 378*(3–4), 299–304.
Kim, J. Y., Jung, J. H., Lee, D. E., & Joo, J. (2002). Enhancement of electrical conductivity of poly(3,4-ethylenedioxythiophene)/poly(4-styrenesulfonate) by a change of solvent. *Synthetic Metals, 126*, 311–316.
Kirk, C. T. (1988). Quantitative analysis of the effect of disorder-induced mode coupling on infrared absorption in silica. *Physical Review B, 38*(2), 1255–1273.
Lee, C., Kang, H., Kim, H., Nguyen, H. A. D., & Shin, K. (2010). Quality control with matching technology in roll to roll printed electronics. *Journal of Mechanical Science and Technology, 24*, 315–318.
Legnani, C., Vilani, C., Calil, V. L., Barud, H. S., Quirino, W. G., Achete, et al. (2008). Bacterial cellulose membrane as flexible substrate for organic light emitting devices. *Thin Solid Films, 517*(3), 1016–1020.
Lewis, J. (2006). Material challenge for flexible organic devices. *Materials Today, 9*(4), 38–45.
Lewis, J. S., & Weaver, M. S. (2004). Thin-film permeation-barrier technology for flexible organic light-emitting devices. *IEEE Journal of Selected Topics in Quantum Electronics, 10*(1), 45–57.
Liew, Y. F., Aziz, H., Hu, N. X., Chan, H. S. O., Xu, G., & Popovic, Z. (2000). Investigation of the sites of dark spots in organic light-emitting devices. *Applied Physics Letters, 77*(17), 2650–2652.
Nogi, M., & Yano, H. (2008). Transparent nanocomposites based on cellulose produced by bacteria offer potential innovation in the electronics device industry. *Advanced Materials, 20*, 1849–1852.
Noh, J., Yeom, D., Lim, C., Cha, H., Han, J., Kim, J., et al. (2010). Scalability of roll-to-roll gravure-printed electrodes on plastic foils. *IEEE Transactions on Electronics Packaging Manufacturing, 33*(4), 275–283.
Okahisa, Y., Yoshida, A., Miyaguchi, S., Yano, H., et al. (2009). Optically transparent wood-cellulose nanocomposite as a base substrate for flexible organic light-emitting diode displays. *Composites Science and Technology, 69*, 1958–1961.
Papadimitrakopoulos, F., Zhang, X. M., & Higginson, K. A. (1998). Chemical and morphological stability of aluminum tris(8-hydroxyquinoline) (Alq(3)): Effects in light-emitting devices. *IEEE Journal of Selected Topics in Quantum Electronics, 4*(1), 49–57.
Sperling, L. H. (2001). *Introduction to Physical Polymer Science*.
Techima, K., Inoue, Y., Sugimura, H., & Takai, O. (2001). Room-temperature deposition of high-purity silicon oxide films by RF plasma-enhanced CVD. *Surface and Coatings Technology, 146–147*, 451–456.
Tendero, C., Tixier, C., Tristant, P., Deamaison, J., & Leprince, P. (2006). Atmospheric pressure plasmas: A review. *Spectrochinica Acta Part B: Atomic Spectroscopy, 61*, 2–30.
Tomita, M., Hashimoto, T., Endoh, H., & Yokota, Y. (1985). Improvement and application of the Fourier-transformed pattern from a small area of high resolution electron microscope images. *Ultramicroscopy, 16*, 9–18.
Wu, C. (2010). *Production and characterization of optically transparent nanocomposite film*. Toronto: University of Toronto.
Wuu, D. S., Lo, W. C., Chang, L. S., & Horng, R. H. (2004). Properties of SiO$_2$-like barrier layers on polyethersulfone substrate by low-temperature plasma-enhanced chemical vapor deposition. *Thin Solid Films, 468*, 105–108.
Yang, Y. J., Jiang, Y. D., Xu, J. H., & Yu, J. S. (2007). Conductive PEDOT-PSS composite films assembled by LB technique. *Colloids and Surfaces A: Physicochemical Engineering Aspects, 302*, 157–161.